Journal of Biomolecular NMR (2005) 33: 105–121
DOI 10.1007/s10858-005-1206-5

Article

Accurate determination of leucine and valine side-chain conformations using U-[^{15}N/^{13}C/^{2}H]/[^{1}H-(methine/methyl)-Leu/Val] isotope labeling, NOE pattern recognition, and methine Cγ–Hγ/Cβ–Hβ residual dipolar couplings: application to the 34-kDa enzyme IIA^{Chitobiose}

Chun Tang, Junji Iwahara & G. Marius Clore*
Laboratory of Chemical Physics, National Institute of Diabetes and Digestive and Kidney Diseases, National Institutes of Health, Building 5/B1-30I, Bethesda, MD, 20892-0520, USA

Received 14 June 2005; Accepted 14 July 2005

Key words: isotope labeling, Leu and Val conformation, NMR, NOE, residual dipolar couplings, solution structure

Abstract

An isotope labeling scheme is described in which specific protonation of methine and methyl protons of leucine and valine is obtained on a ^{15}N/^{13}C labeled background with uniform deuteration of all other non-exchangeable protons. The presence of a protonated methine group has little effect on the favorable relaxation properties of the methyl protons of Leu and Val. This labeling scheme permits the rotameric state of leucine side-chains to be readily determined by simple inspection of the pattern of Hγ(i)–H_N(i) and Hγ(i)–H_N(i + 1) NOEs in a 3D ^{15}N-separated NOE spectrum free of complications arising from spectral overlap and spin-diffusion. In addition, one-bond residual dipolar couplings for the methine ^{13}C–^{1}H bond vectors of Leu and Val can be accurately determined from an intensity J-modulated constant-time HCCH-COSY experiment and used to accurately orient the side-chains of Leu and Val. Incorporation of these data into structure refinement improves the accuracy with which the conformations of Leu and Val side-chains can be established. This is important to ensure optimal packing both within the protein core and at intermolecular interfaces. The impact of the method on protein structure determination is illustrated by application to enzyme IIA^{Chitobiose}, a 34 kDa homotrimeric phosphotransferase protein.

Introduction

Buried methyl side-chains play a major role in packing the hydrophobic core of proteins, thereby stabilizing the native protein fold, while surface methyl groups contribute significantly to van der Waals interactions at protein–protein, protein–nucleic acid and protein–ligand interfaces (Lo Conte et al., 1999). Indeed, leucine residues generally make up over 10% of the intermolecular interface in oligomeric proteins (Lo Conte et al., 1999). In this regard, chemical shift perturbation of Ile, Leu and Val methyl groups has proved to be a powerful tool in NMR-based ligand screening (Hajduk et al., 2000). Moreover, NOEs involving only methyl and backbone amide groups, in conjunction with torsion angle and backbone residual dipolar couplings, can be used to determine accurate three-dimensional solution structures of proteins, as recently demonstrated by the structure determination of the 34-kDa enzyme IIA^{chitobiose} (IIA^{Chb}) homotrimer which comprises a leucine

*To whom correspondence should be addressed. E-mail: mariusc@intra.niddk.nih.gov

coiled-coil at the trimer interface (Tang et al., 2005). Further, conformational plasticity of interfacial side-chains plays an important role in protein-target recognition (Betts and Sternberg, 1999; Najmanovich et al., 2000; Wang et al., 2000). Thus, the precise and accurate delineation of the conformations of methyl bearing side-chains can have a large impact on the quality of the structures of proteins and their complexes determined by NMR spectroscopy.

NMR structure determination has largely been based on semi-quantitative NOE-derived interproton distance restraints supplemented by loose torsion angle restraints obtained from a combination of J coupling and NOE analysis (Wüthrich, 1986; Clore and Gronenborn, 1989). While extremely powerful, this approach is relatively insensitive to subtle conformational changes, particularly for side-chains. Residual dipolar couplings (RDC) measured in weakly aligned systems offer a means for obtaining accurate quantitative information in the form of bond vector orientations relative to an alignment tensor (Tolman et al., 1995; Tjandra and Bax, 1997; Tjandra et al., 1997; Prestegard et al., 2000; Bax et al., 2001). Much of the published work has focused on backbone RDCs and relatively few attempts have been made to measure RDCs for side-chain bond vectors. Experiments have been devised to measure RDCs for methyl ^{13}C–^{1}H vectors (Ottiger et al., 1998; Kontaxis and Bax, 2001; Sibille et al., 2002) and ^{13}C–^{13}C vectors (Permi et al., 2000; Evenas et al., 2001; Vögeli et al., 2004), as well as the sum of the RDCs for the two ^{13}C–^{1}H vectors of methylene groups (Ottiger et al., 1998; Chou and Bax, 2001; Mittermaier and Kay, 2001). In addition, RDCs have been reported for side-chain amides of Asn and Gln (Cai et al., 2001; Permi, 2001; Higman et al., 2004). Nevertheless, these experiments have found little if no application in actual structure determinations, in part because of their complexity (both in terms of the pulse sequences and the data analysis), as well as problems associated with spectral overlap, particularly with increasing size and complexity of the system under investigation.

In this paper, we present a simple and straightforward approach for the accurate determination of leucine and valine side-chain conformations and demonstrate its utility on the 34-kDa coiled-coil homotrimeric phosphotransferase enzyme IIA^{Chb}. The approach is based on an isotope labeling scheme in which the protein is uniformly labeled with ^{15}N, ^{13}C and all non-exchangeable hydrogens are replaced by deuterons with the exception of the side-chain methine and methyl protons of Leu and Val. With the present labeling scheme, the χ_1/χ_2 rotamers of Leu can be readily derived from the pattern of intraresidue H_N–Hγ and sequential interresidue Hγ(i)–H_N(i + 1) NOEs, making *a priori* stereospecific assignments of the Leu prochiral methyl groups unnecessary. In addition, the RDCs for the Leu Cγ–Hγ and Val Cβ–Hβ bond vectors can be readily and accurately measured and used to optimally orient the methyl-bearing side-chains of Leu and Val.

Experimental

Protein expression and isotopic labeling

IIA^{Chb}-NΔ13/D92L, also known as IIA^{Chb}* (in which the disordered N-terminal tail is deleted and the Asp to Leu mutation at position 92 ensures the formation of a monodisperse trimer), was expressed in BL21-Star cells as described previously (Tang et al., 2005). Cells were grown in M9 minimal medium prepared in D_2O with [$^{2}H_7$, $^{13}C_6$]-glucose and [^{15}N]-NH_4Cl as the carbon and nitrogen sources, respectively. Eighty mg [$^{13}C_5$]-α-ketoisovalerate (purchased from Cambridge Isotopes, Andover, MA) was added to 1 L culture 45 min prior to induction. Protein expression was induced with 1 mM isopropyl-β-D-thiogalactopyranoside (IPTG) at an $OD_{600\ nm}$ of 0.8. IIA^{Chb}* was purified by anion exchange and size exclusion chromatography as described (Tang et al., 2005). Typically 1 mM protein was prepared in 90% H_2O/10% D_2O containing 10 mM sodium phosphate buffer, pH 6.5 and 0.02% NaN_3. The NMR sample is uniformly ^{15}N and ^{13}C labeled, and is fully deuterated except for the backbone and side-chain amides, the γ-methine and δ-methyls of Leu, and the β-methine and γ-methyls of Val which are protonated. For residual dipolar coupling measurements the protein was aligned in 22 mg/ml phage pf1 (Clore et al., 1998; Hansen et al., 1998).

NMR spectroscopy

NMR spectra were recorded at 30 °C on a Bruker DRX800 spectrometer equipped with a z-shielded

gradient triple resonance cryoprobe. Spectra were processed and analyzed with the NMRPipe/nmrDraw suite (Delaglio et al., 1995). NOEs between backbone amide protons and methine/methyl protons of Leu and Val were obtained from a 3D TROSY-based (Peruvshin et al., 1997) ^{15}N-separated NOE experiment. Backbone $^{1}J_{NH}$ couplings were measured from splittings in a 3D HNCO-TROSY-based experiment (Yang et al., 1999). Methine $^{1}J_{CH}$ couplings were measured from a series of intensity J-modulated 3D HCCH-COSY constant time experiments as described in the Results.

Structure calculations

Structures were calculated from the experimental NMR restraints by simulated annealing in torsion angle space (Schwieters and Clore, 2001b) using the program Xplor-NIH (Schwieters et al. 2003). The experimental restraints comprise the NOE-derived interproton distance restraints, backbone and side-chain torsion angle restraints, and backbone $^{1}D_{NH}$, $^{1}D_{NC'}$ and $^{1}D_{C\alpha C'}$ RDCs published previously (Tang et al., 2005), supplemented by the current set of Leu side-chain torsion angle restraints and RDCs for the Cγ–Hγ and Cβ–Hβ bond vectors of Leu and Val, respectively. The NMR restraints thus comprise: 276×3 interproton distance restraints (including 78×3 ambiguous inter-subunit restraints); 154×3 distance restraints for 77 backbone hydrogen bonds per subunit; 243×3 torsion angle restraints (including 73×3 side-chain torsion angle restraints), 100×3 ^{13}Cα and 95×3 ^{13}Cβ chemical shift restraints; 84×3 $^{1}D_{NH}$, 85×3 $^{1}D_{NC'}$ and 83×3 $^{1}D_{C\alpha C'}$ backbone RDC restraints; and from this work 18×3 $^{1}D_{CH}$ Val and Leu side-chain methine RDC restraints (cf. Table 1). The non-bonded contacts in the target function were represented by a quartic van der Waals repulsion term (Nilges et al., 1988) supplemented by a radius of gyration term (Kuszewski et al., 1999), and multi-dimensional torsion angle (Clore and Kuszewski, 2002) and hydrogen bonding database potentials of mean force (Grishaev and Bax, 2004). Each set of calculations comprised 100 simulated annealing structures. There are no NOE violations >0.3 Å or torsion angle violations $>5°$. The r.m.s. deviations from the distance, torsion angle, and ^{13}Cα and ^{13}Cβ chemical shift restraints are 0.009 ± 0.003 Å, $0.24 \pm 0.05°$, 1.13 ± 0.02 ppm and 0.64 ± 0.02 ppm, respectively. The dipolar coupling R-factors (Clore and Garrett, 1999) for the backbone $^{1}D_{NH}$, $^{1}D_{NC'}$ and $^{1}D_{C\alpha C'}$ RDCs are $6.93 \pm 0.08\%$, $17.8 \pm 1.0\%$ and $15.8 \pm 1.0\%$, respectively. The dipolar coupling R-factor for the Val and Leu side-chain methine $^{1}D_{CH}$ RDCs is $2.1 \pm 0.2\%$ for the structures calculated using a harmonic potential for the side-chain RDCs and $40.7 \pm 3.2\%$ for the structures calculated without $^{1}D_{CH}$ RDCs. The deviations from idealized bond lengths, bond angles and improper torsions are 0.002 ± 0 Å, $0.39 \pm 0.01°$ and $0.57 \pm 0.04°$, respectively. The coordinate precision, defined as the average atomic r.m.s. difference between the individual 100 simulated annealing structures and the corresponding mean coordinates obtained by best-fitting residues 17–73 and 83–114 of all three subunits simultaneously, is 0.28 Å for the backbone and 0.80 Å for all heavy atoms. (Note that the first residue of the IIA^{Chb*} constructs is numbered 14, and residues 14–16, 74–82 and 115–116 are disordered in solution). The percentage for residues in the most favored region of the Ramachandran map is $93.9 \pm 1.5\%$. Structures were displayed using the program VMD-XPLOR (Schwieters and Clore, 2001a).

Results and discussion

Selective proton labeling of side-chain methine and methyl protons of Leu and Val

The selective isotope labeling strategy we employed is designed to selectively protonate the γ-methine and δ-methyls of Leu and the β-methine and γ-methyls of Val biosynthetically on an otherwise fully deuterated background with uniform ^{15}N and ^{13}C labeling. To this end, [$^{13}C_5$]-α-ketoisovalerate was added to M9 minimal medium in D_2O containing [$^{13}C_6$,$^{2}H_7$]-glucose and $^{15}NH_4Cl$ as the carbon and nitrogen sources, respectively. This differs from the labeling scheme described by Kay and coworkers (Goto et al., 1999), in which [$^{13}C_5$, 3–$^{2}H_1$]-α-ketoisovalerate was used as the biosynthetic precursor for Leu and Val, resulting in protonation of methyl groups but deuteration of the methine positions. The 3-methine proton of α-ketoisovalerate is slightly acidic due to interconversion between the keto and enol isomers. As deuterium exchange which converts [$^{13}C_5$]-α-ketoisovalerate to [$^{13}C_5$, 3–$^{2}H_1$]-α-ketoisovalerate is

Table 1. Rotamer assignments and RDCs for Val and Leu residues of IIA^{Chb*}

		Normalized RDCs (Hz)[a]		
	χ_1/χ_2	Methine $^1D_{CH}$[b]	$^1D_{C\alpha(i-1)-C'(i-1)}$	$^1D_{C\alpha(i)-C'(i)}$
Valine[c]				
V20	*t*	−12.4 ± 1.7	−24.0	−4.1
V21	*t*	d	−4.1	−7.1
V67	*t*	−15.8	−54.2	11.2
V83	e	−1.9 ± 0.2	2.3	−4.6
V86	*t*	−7.6 ± 0.8	−3.8	−39.8
V88	*t*	d	−5.1	6.7
Leucine				
L17	g^-/t	−21.0 ± 0.9	−17.3	7.4
L24	g^-/t	−22.3	−8.5	12.0
L34	g^-/t	9.1 ± 2.1	g	−7.8
L39	t/g^+	10.4 ± 3.5	−11.8	8.1
L61	g^-/t	f	g	g
L66	g^-/t	−5.9	−6.1	−54.2
L71	g^-/t	−5.7	−20.0	18.6
L85	e	0.2 ± 1.9	g	−3.8
L87	g^-/t	−13.1 ± 0	−39.8	−5.1
L92	t/g^+	3.5	−8.6	−16.0
L94	g^-/t	−4.8 ± 0.3	−2.5	−8.1
L99	t/g^+	−17.7	−14.8	−21.4
L103	g^-/t	−15.6 ± 0.4	−21.2	−8.2
L107	g^-/t	f	0.3	−1.5
L110	g^-/t	14.8 ± 1.4	−9.7	−4.4
L114	g^-/t	−1.4 ± 0.6	−9.7	−3.0

[a]The backbone Cα–C′ RDCs (taken from Tang et al., 2005) are normalized to those of the methine C–H RDCs on the basis of bond length, gyromagnetic ratio and the magnitude of the axial component of the alignment tensor (D_a). (Note the alignment tensor for a trimer is axially symmetric, i.e. $\eta = 0$; Al-Hashimi et al., 2000). The value of D_a^{NH} for the current data, recorded in 22 mg/ml phage pf1, is −17.8 Hz (i.e. $D_a^{NH} = -36.1$ Hz); this value was determined by linear regression between the backbone N–H RDCs measured for the current sample and those previously measured for the NMR structure determination which were recorded in 15 mg/ml phage. The value of $D_a{}^{NH}$ for the latter, determined from a histogram of the measured backbone RDCs, is −12.1 Hz (Tang et al., 2005). The dipolar coupling *R*-factor (Clore and Garrett, 1999) for the current set of N–H RDCs when best-fitted to the coordinates of the original restrained regularized mean NMR structure is 6.9%. This compares to a value of 7.1% for the original set of N–H RDCs that were used directly in the NMR structure determination (Tang et al., 2005).

[b]The average value and standard deviation are given in those instances where the $^1D_{CH}$ coupling could be measured independently from the two methyl cross-peaks. When no standard deviation is given, $^1D_{CH}$ was obtained from only a single measurement, either because one of the two methyl cross-peaks was overlapped with that of another residue or because the two methyl groups had degenerate ^1H chemical shifts. The uncertainties in the values of $^1D_{CH}$ derived by Monte Carlo analysis of the errors in the fitted values of $^1J_{CH}$, are generally less than 2 Hz (see text).

[c]The rotamer assignments for the Val residues were derived from $^3J_{NC_\gamma}$ and $^3J_{C'C_\gamma}$ couplings measured by quantitative J correlation spectroscopy.

[d]The Cβ–Hβ RDCs for Val 21 and Val88 could not be measured due to spectral overlap.

[e]Val83 and Leu85 are rotamer averaged.

[f]The Cγ–Hγ RDCs for Leu61 and Leu103 could not be measured due to weak cross-peak intensities in the intensity J-modulated HCCH-COSY spectra for the aligned state.

[g]Cα-C′ RDCs could not be determined for Ser33, Leu34, Ala60, Leu61, and Ser84.

only accelerated by basic pD or pH* (Goto et al., 1999), the 3-methine proton is relatively stable at neutral pH*. Referenced to the ^1H resonance of the methyl protons of α-ketoisovalerate, the peak intensity for the 3-methine proton resonance remains unchanged when incubated overnight in D_2O buffer at neutral pH* and 37 °C (data not shown). *In vivo*, α-ketoisovalerate is rapidly

converted to Val and 3-carboxy-3-hydroxy-isocaproate, a more immediate precursor of Leu (*E. Coli* Metabolism Pathway Database http://biocyc.org). As a result, the 3-methine proton of α-ketoisovalerate loses its acidity and the potential to exchange to a deuteron. Consequently, when [$^{13}C_5$]-α-ketoisovalerate is used as the biosynthetic precursor for protein expression in D_2O minimal medium, almost the same levels of protonation can be obtained for the side-chain methines as for the methyl groups of Leu and Val.

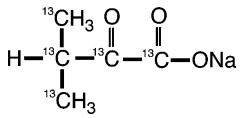

Contribution of methine protons to the relaxation of Leu/Val methyls

For macromolecules, the transverse (R_2) relaxation rate is dominated by the spectral density at zero-frequency. Thus, the additional contribution to methyl proton relaxation of Leu and Val as a consequence of intraresidue dipolar interactions with the methine proton is given by:

$$R_2^{DD} = \frac{1}{4}\left(\frac{\mu_0}{4\pi}\right)^2 \hbar^2 \gamma_H^4 \tau_c \left\langle r_{H-H}^{-3}\right\rangle^2 \left\langle P_2(\cos\chi_{ij})\right\rangle \quad (1)$$

where r is the distance between the side-chain methine and methyl protons, μ_0 the vacuum permeability ($4\pi\times10^{-7}$ kg m s^{-2} A^{-2}), $\hbar$ Planck's constant divided by 2π (1.0546×10^{-34}J · s · rad^{-1}), γ_H the proton gyromagnetic ratio (2.6752×10^8 rad · s^{-1} · T^{-1}), and τ_c the rotational correlation time (estimated at 15 ns for a 34 kDa globular protein); $P_2(\cos\chi_{ij})$ is the second-order Legendre polynomial $(3\cos^2\chi_{ij} - 1)/2$ where χ_{ij} is the angle between the Leu Hγ–Hδ or Val Hβ–Hγ vectors i and j in the three site discrete jump model of methyl rotation (Bruschweiler and Case, 1994). For fixed atoms in the molecular frame, the average values for the effective distance $< r^{-3} >^{-1/3}$ and P_2 function are 2.6 Å and 0.62, respectively. From Eq. (1) the additional contribution to methyl proton relaxation by the methine proton is calculated to be less than 4 s^{-1}, compared to an average transverse relaxation rate R_2 of 28 s^{-1} measured for the methyl protons of Leu and Val in a U-[^{15}N/^{13}C/^{2}H]/[Leu/Val/Ile-methyl-protonated] sample of IIA^{Chb}* (Tang et al., 2005). Indeed, a high quality methyl-TROSY ^{1}H–^{13}C HMQC spectrum can still be obtained for ^{15}N/^{13}C/^{2}H/(Leu/Val-methine/methyl-protonated) IIA^{Chb}* at 5 °C (data not shown). Thus, the favorable relaxation properties of the methyl protons of Leu and Val are largely preserved, thereby readily allowing the implementation of sensitive experiments for methyl-detected, methine ^{13}C–^{1}H vector RDC measurements.

Assignment of Leu side-chain rotamers based on NOE patterns involving the H_N and Hγ protons

Leu side-chain rotamers can readily be deduced from the pattern of intraresidue Hγ(i)–H_N(i) and sequential interresidue Hγ(i)–H_N(i + 1) NOE cross-peak intensities observed in a 3D TROSY-based ^{15}N-separated NOE spectrum recorded on a ^{15}N/^{13}C/^{2}H/(Leu/Val-methine/methyl-protonated) sample. The deuterated background eliminates spectral overlap (particularly with the Hβ protons of Leu); improves the relaxation properties of the Hγ methine proton that generally relaxes faster than the rotating methyl protons; and renders the analysis simple by eliminating spin-diffusion pathways from the H_N to Hγ protons. The latter also enables longer mixing times to be used. Analysis of high-resolution crystal structures reveals that the distribution of Leu χ_1/χ_2 torsion angles is coupled, and that Leu side-chains adopt almost exclusively two conformations: g^-/t and t/g^+ (Karplus, 1996; Kuszewski et al., 1996). Note that the χ_1 g^+ rotamer for Leu is never found. For a given χ_1/χ_2 rotamer, the Hγ(i)–H_N(i) intraresidue distance is only dependent on the backbone torsion angle φ, while the interresidue Hγ(i)–H_N(i + 1) distance depends only on ψ. In the g^-/t rotamer, the Hγ(i)–H_N(i) distance is shorter than the Hγ(i)–H_N(i + 1) distance for all commonly occurring Leu ϕ/ψ backbone torsion angles (Figure 1a), while for t/g^+ rotamer the Hγ(i)–H_N(i + 1) distance is generally shorter than or comparable to the Hγ(i)–H_N(i) distance (Figure 1b). As the secondary structure classification and ϕ/ψ angles can be derived from backbone chemical shifts (Cornilescu et al., 1999), Leu side-chain rotameric state can be readily deduced from the pattern of Hγ–H_N NOEs.

By comparing intraresidue and interresidue Hγ–H_N NOE cross-peak intensities, we were able

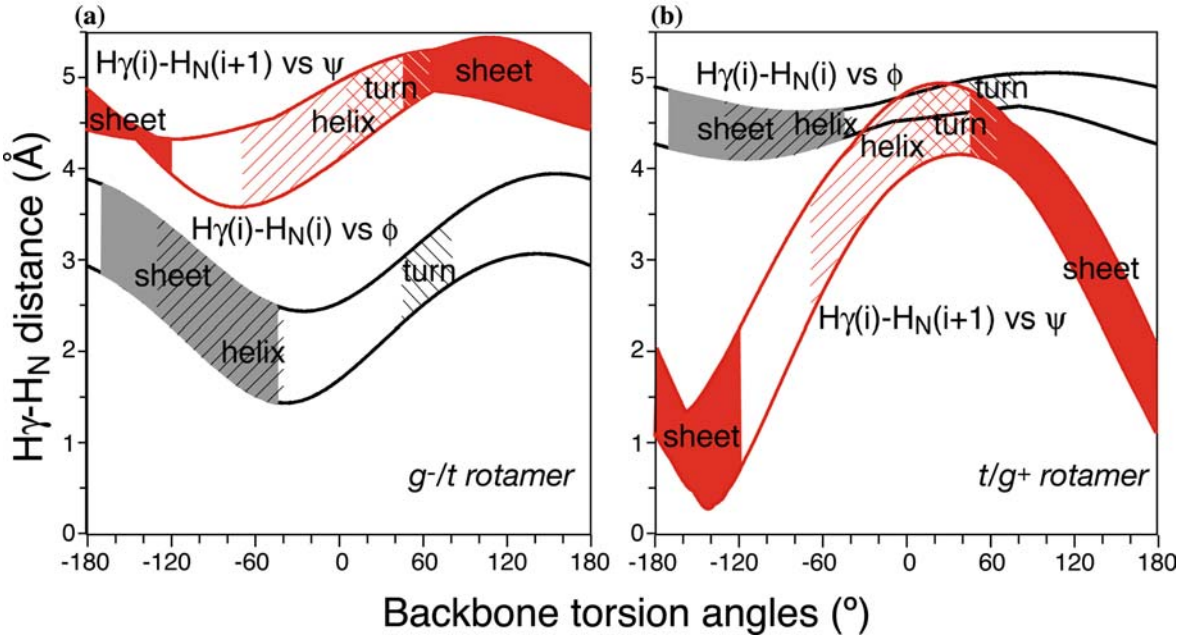

Figure 1. Backbone ϕ/ψ dependence of the distance between the Leu Hγ proton and either its own or the following backbone amide proton. For a given χ_1/χ_2 rotameric state, $r_{H\gamma(i)-HN(i)}$ is only dependent on ϕ (black), and $r_{H\gamma(i)-HN(i+1)}$ is only dependent on ψ (red). The maximum and minimum Hγ–H_N distances are calculated without considering van der Waals repulsion from a set of conformations within 20° of ideally staggered rotamers. All commonly occurring Leu ϕ/ψ angles are labeled according to their corresponding secondary structures. Regions in white are not sampled by leucine residues in high-resolution protein crystal structures. The g^-/t rotamer is shown in (a), and the t/g^+ state is shown in (b).

to obtain rotamer assignments for 15 out of a total 16 Leu residues in IIA^{Chb}* (Table 1). Twelve Leu residues adopt the g^-/t rotamer, and 3 residues, including Leu39, Leu92 and Leu99, adopt the t/g^+ rotamer. This finding is fully consistent with statistics from the protein structure database that indicate that the g^-/t rotamer is the most populated Leu conformation (Conformational Angle Database at http://cluster.physics.iisc.ernet.in/cadb). Representative strips from a 70 ms mixing time 3D ^{15}N-separated NOE experiment illustrating the rotamer assignments for Leu34 and Leu92 are shown in Figure 2. In the case of Leu34, a strong intraresidue Hγ(i)–H_N(i) cross-peak is observed and no sequential Hγ(i)–H_N(i + 1) NOE is seen, indicative of the g^-/t rotamer (Figure 2a). For Leu92, on the other hand, only a sequential Hγ(i)–H_N(i + 1) cross-peak is observed indicative of the t/g^+ rotamer (Figure 2b). The only Leu residue for which we were unable to assign the rotameric state was Leu85 as no cross-peaks were observed between its Hγ proton and the backbone amide of either its own or the following residue. This is consistent with the fact that Leu85, which is located at the N-terminus of α-helix 3, is rotamer averaged (Tang et al., 2005).

The Leu rotamer assignments derived from a qualitative interpretation of the H_N–Hγ NOE cross-peak intensities are given in Table 1 and are in agreement with those obtained from analysis of ^{3}J couplings. However, the latter requires more complicated pulse sequences (a combination of N–Cγ and ^{13}C–^{13}C long-range quantitative J correlation experiments) and data analysis (Bax et al., 1992; Hu and Bax, 1997; Konrat et al., 1997), and in the case of IIA^{Chb}* yielded less than half of the Leu rotamer assignments due to spectral overlap. Thus, the qualitative interpretation of the pattern of Hγ(i)–H_N(i) and Hγ(i)–H_N(i + 1) NOEs offers a complementary approach to J-coupling measurements for establishing the Leu rotamer assignment. For the purposes of structure calculation there is no need to convert the H_N–Hγ NOEs into approximate, loose interproton distance ranges since the latter would be of relatively little value; rather these NOEs can be directly translated into Leu χ_1/χ_2 side-chain torsion angle restraints represented by square-well potentials with widths

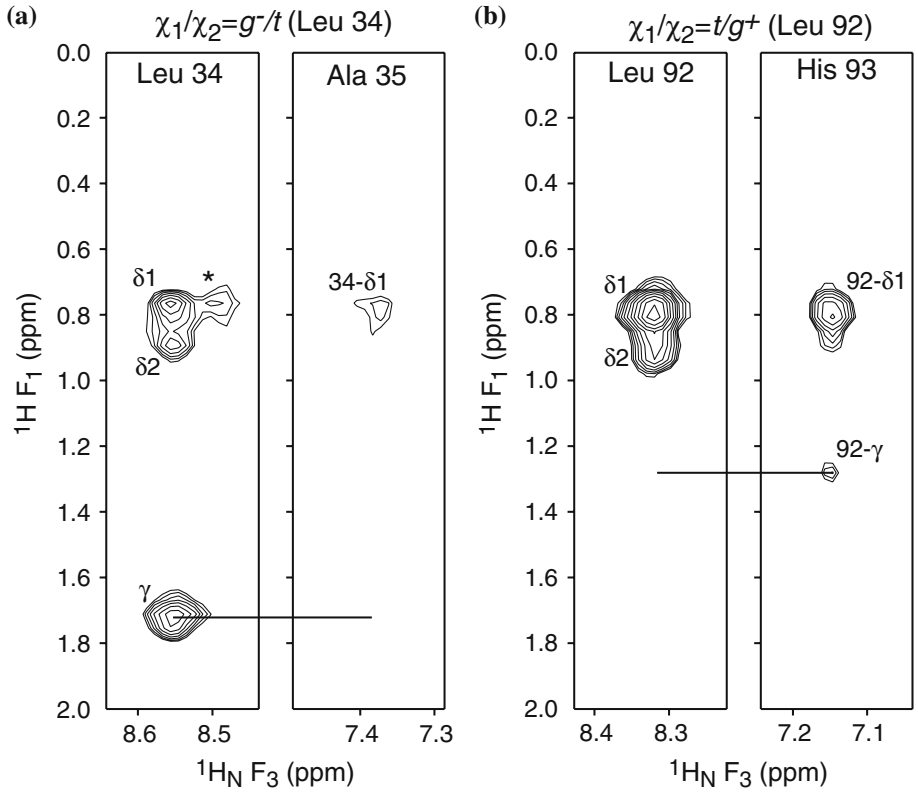

Figure 2. Representative strips taken from a 70 ms mixing time 3D TROSY-based ^{15}N-separated NOE spectrum recorded on U-[^{15}N/^{13}C/^{2}H]/[Leu/Val-methine/methyl-protonated] labeled IIA^{Chb}*. Only the proton aliphatic region between 0 and 2 ppm is shown. Strips for residues Leu34 and Ala35 are shown in (a), and strips for Leu92 and His93 and shown in (b). The methyl and Hγ protons are labeled and the asterisk denotes a cross-peak from an adjacent plane.

of $\pm 20°$ for χ_1 and $\pm 30°$ for χ_2, centered around 180°, $-60°$ and $+60°$ for the *t*, g^- and g^+ rotamers, respectively.

Once the Leu side-chain rotamers are assigned and the information incorporated in the form of χ_1/χ_2 torsion angle restraints, the two prochiral methyl groups will be automatically spatially differentiated during the course of the structure calculations, thereby making it unnecessary to obtain stereospecific assignments *a priori*. In this sense, the information content afforded by the combination of ambiguous, non-sequential NOE-derived interproton restraints (in the form of a single $(\sum_{ij} r_{ij}^{-6})^{-1/6}$ sum representation for the NOEs involving the two methyl groups of a given Leu) acting in concert with χ_1/χ_2 side-chain torsion angle restraints (which confine the Leu side-chain to a single χ_1/χ_2 rotamer) is conformationally more restrictive than that afforded by individual distance restraints for each methyl group. This is particularly so as the quality of the latter are easily degraded by spin-diffusion between the two prochiral methyl groups.

Side-chain RDC measurement for Leu Cγ–Hγ and Val Cβ–Hβ bond vectors

RDCs for Leu Cγ–Hγ and Val Cβ–Hβ bond vectors were measured on the ^{15}N/^{13}C/^{2}H/(Leu/Val-methine/methyl-protonated) sample of IIA^{Chb}* using an intensity J-modulated 3D constant time HCCH-COSY experiment (Figure 3). Water suppression and the coherence transfer pathway are based on the gradient-enhanced HCCH-TOCSY experiment previously described (Kay et al., 1993). As magnetization can start from either the methine or methyl protons of Leu and Val, the pulse sequence was optimized to favor coherence transfer from the methine (Leu Hγ and Val Hβ) to methyl (Leu Hδ

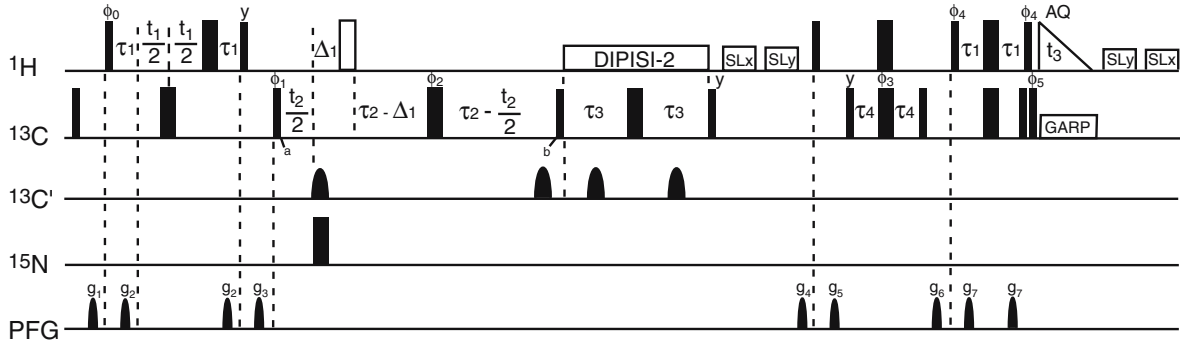

Figure 3. Intensity-modulated 3D HCCH-COSY pulse sequence for measuring one-bond methine ^{13}C–^{1}H J couplings for Leu and Val side-chains. The data were collected in an interleaved mode with three different Δ_1 delays (0.6, 3.0 and 3.6 ms) obtained by moving the position of the 180° ^{1}H pulse indicated by the wide open rectangle. The other delays are: $\tau_1 = 1.8$ ms, $\tau_2 = 3.9$ ms, $\tau_3 = 7.1$ ms and $\tau_4 = 0.6$ ms. Narrow and wide pulses have flip angles of 90° and 180°, respectively. Shaped 180° pulses on $^{13}C'$ were applied as sinc pulses with a maximum field strength of 5.7 kHz. Homogeneity spoiler (SL) pulses for water suppression were applied at 5 kHz field for 4 ms. A 5 kHz field strength was employed for ^{1}H DIPSI-2 decoupling during the $2\tau_3$ period. z-axis pulse field gradients are g_1, g_2 and g_7, 0.4 ms at 20 G/cm; g_3, 2 ms at −25 G/cm; g_4, 3.8 ms at 30 G/cm; g_5, 2.8 ms at −15 G/cm; and g_6, 2.8 ms at 30 G/cm. The phase cycling is: $\phi_0 = x$, $\phi_1 = (x, -x)$, $\phi_2 = (2x, 2y)$, $\phi_3 = (4x, 4y)$, $\phi_4 = (x, y, -x, -y)$, $\phi_5 = (4x, -4x)$, and receiver phase (x, y, x, y, $-x$, $-y$, $-x$, $-y$). Quadrature-detection for the $^{1}H(F_1)$ and $^{13}C(F_2)$ dimensions was achieved by using States-TPPI on ϕ_0 and ϕ_1, respectively.

and Val Hγ) protons. The pathway can therefore be depicted as Hγ → Cγ → Cδ → Hδ for Leu and Hβ → Cβ → Cγ → Hγ for Val. Modifications in the HCCH-COSY pulse sequence include: (1) setting the delay τ_3 to 7.1 ms to selectively refocus the ^{13}C–^{13}C anti-phase term on ^{13}C methyl carbon which is bonded to only one ^{13}C atom; and (2) setting the delay τ_4 to 0.6 ms to maximize coherence transfer from the methyl carbon to methyl protons in a IS_3 type spin system.

For the purposes of simplification, we will mainly discuss magnetization transfer in the case of Leu. Following the first INEPT transfer at point *a* of the pulse sequence (Figure 3), the product operator can be written as $2H_z^{\gamma}C_y^{\gamma}$ for Leu, and the product operator at point *b* that gives rise to observable (Hγ, Cγ, Hδ1) cross-peaks can be denoted as:

$$2C_y^{\gamma}C_z^{\delta 1}\cos(\pi J_{C\beta C\gamma}2\tau_2)\times\cos(\pi J_{C\delta 2C\gamma}2\tau_2)\times\sin(\pi J_{C\delta 1C\gamma}2\tau_2)\times\sin(\pi J_{C\gamma H\gamma}2\Delta_1) \quad (2)$$

As a result of one-bond carbon–carbon scalar couplings to Cγ ($^{1}J_{C\beta C\gamma}$, $^{1}J_{C\delta 2C\gamma}$ and $^{1}J_{C\delta 1C\gamma}$), the term $\cos(\pi J_{C\beta C\gamma}2\tau_2)\times\cos(_{C\delta 2C\gamma}2\tau_2)\times\sin(\pi J_{C\delta 1C\gamma}2\tau_2)$ reaches its maximum at ~2.8 ms. τ_2, however, was set to 3.9 ms to increase the resolution in the carbon dimension at a cost of an approximately 15% loss in signal intensity. It should be noted that even though the digital resolution in the ^{13}C (F_2) dimension is limited by a total acquisition time of $2\tau_2$, it is more than sufficient to resolve all the Leu Cγ/Val Cβ chemical shifts. Following a similar path, Cγ magnetization is transferred to the $C\delta_2$-methyl carbon and equally strong cross-peaks for the two methyl groups are associated with every Hγ–Cγ coupling (Figure 4a). Elimination of Leu $^{1}J_{C\gamma-C\beta}$ and Val $^{1}J_{C\beta-C\alpha}$ evolutions by appropriate selective ^{13}C 180° pulses could potentially improve sensitivity, but this would require long shaped pulses that could introduce additional Cγ–Hγ/Cβ–Hβ coupling evolution that could not be precisely accounted for. Most importantly, as defined in Eq. (2), the final signal intensity is sinusoidally modulated for a given Cγ–Hγ ^{1}J coupling. Therefore the $^{1}J_{C\gamma-H\gamma}$ coupling constant for Leu (and the $^{1}J_{C\beta-H\beta}$ coupling constant for Val) can be extracted by fitting the signal intensities at different $2\Delta_1$ delays to a sinusoidal curve.

The HCCH-COSY cross-peak intensities for three different J-coupling evolution periods ($2\Delta_1 = 1.2$, 6.0 and 7.2 ms) were quantitated and analyzed using the NMRPipe/nmrDraw suite (Delaglio et al., 1995), yielding excellent fits. The three delays employed give rise to data points removed from the maximum of the sinusoidal curve resulting in larger first derivatives and higher sensitivity for the fitting procedure (Figure 4b).

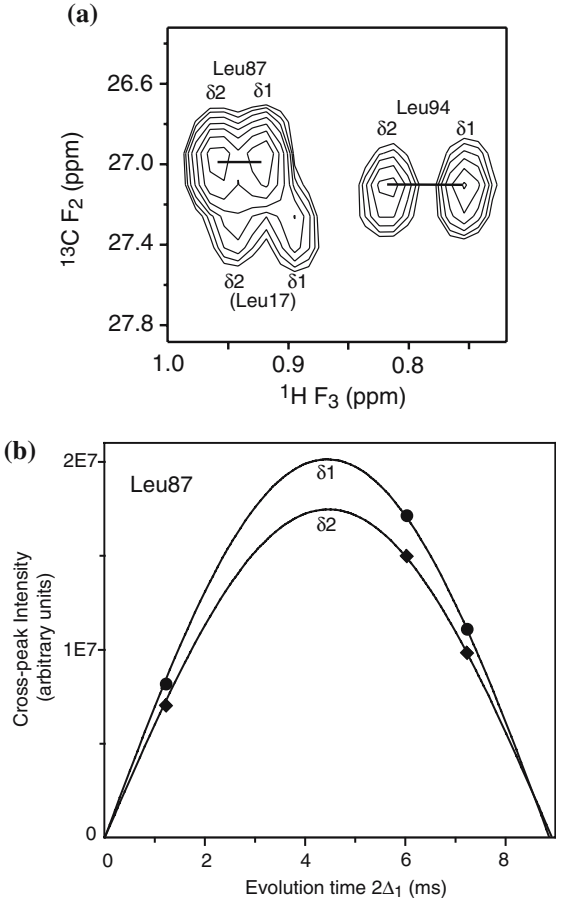

Figure 4. Intensity J-modulated 3D HCCH-COSY experiment recorded on U-[^{15}N/^{13}C/^{2}H]/[Leu/Val-methine/methyl-protonated] labeled IIA^{Chb}* aligned in phage pf1. (a) ^{13}C(F$_2$)–^{1}H(F$_3$) plane at ^{1}H(F$_1$) = 1.65 ppm, illustrating cross-peaks for Leu87 and Leu94 obtained for a $2\Delta_1$ delay of 6.0 ms. The peaks arising from Leu17, which have their maximum on an adjacent plane, are also labeled. The spectrum is a result of a 64 complex (t_1)×15 complex (t_2)×575 complex (t_3) data matrix. The acquisition times in the t_1, t_2 and t_3 dimensions are 33.3, 7.46 and 60 ms, respectively; the sweep widths employed in the t_1, t_2 and t_3 dimensions are 2.40, 10.05 and 12.02 ppm respectively with the carrier frequencies set to 1.2, 30 and 1.2 ppm, respectively. (b) Dependence of the intensities of both methyl cross-peaks of Leu87 as a function of the J-coupling evolution period $2\Delta_1$. Non-linear least squares fitting to a sinusoidal function yields an observed one-bond Cγ–Hγ coupling ($^{1}J_{C-H}+^{1}D_{C-H}$) of 112.82. ± 0.37 Hz from the δ1 methyl curve and 112.19. ± 0.45 Hz from the δ2 methyl curve.

The side-chain Leu Cγ–Hγ and Val Cβ–Hβ RDCs, expressed as the difference between the measured values for the aligned and isotropic states, are listed in Table 1. The fitting errors are principally a function of cross-peak intensities and were estimated by Monte Carlo analysis: the 5%–95% uncertainty limits on the values of the methine $^{1}D_{CH}$ RDCs ranged from ± 0.3 to ± 2.7 Hz, with an average uncertainty of ± 0.9 Hz (which is equivalent to ± 0.45 Hz when normalized relative to the N–H RDCs). For a 34 kDa protein, this degree of precision is entirely reasonable. As the experiment measures the Leu and Val methine $^{1}J_{CH}$ couplings by detection on the methyl protons, the methyl groups of each Leu/Val residue provide two independent measurements of the methine $^{1}J_{CH}$ coupling when the two prochiral methyls can be resolved in the proton acquisition dimension (F_3). Hence, the experimental error is further reduced by averaging the two independent values obtained for each methine $^{1}J_{CH}$ coupling in a single experiment. The average R-factor error (Clore and Schwieters, 2004), given for an axially symmetric system by $100(\mathrm{rmsd})/\sqrt{3.2(D_a^{CH})^2}$ (Al-Hashimi et al., 2000), where rmsd is the root mean square difference between the two sets of RDCs, is ~4%. If the ^{1}H shift of one of the two methyl groups overlaps with that of another residue, or the two methyl groups have degenerate ^{1}H chemical shift, the methine group ^{1}J coupling can still be obtained, albeit with slightly larger experimental error.

The availability of two independent measurements for the Leu $^{1}J_{CH}$ coupling also reveals that the Hγ–Cγ–Hδ cross-peak intensity remains sinusoidally modulated by the Cγ–Hγ ^{1}J coupling in the case of strong coupling between Leu Cγ and Cδ1(2)($\Delta\delta < 5 \times {}^{1}J_{C\gamma C\delta 1(2)}$). Thus, for example, Cγ and Cδ1 of Leu103 are strongly coupled (0.5 ppm chemical shift difference), whereas Cγ and Cδ2 are weakly coupled (4 ppm chemical shift difference). Fitting the sinusoidal modulation of the Hγ–Cγ–Hδ1 and Hγ–Cγ–Hδ2 cross-peaks yields essentially the same value of the Cγ–Hγ ^{1}J coupling (with a good χ^2/N and negligible residuals). One can therefore conclude that refocusing of the antiphase Cγ term with respect to Hγ which occurs during the same period as coherence transfer from Cγ to Cδ is not significantly affected by strong coupling between Cγ and Cδ. The intensity of the Hγ–Cγ–Hδ1 cross-peak of Leu103, however, is only about 60% of that of the Hγ–Cγ–Hδ2 cross-peak, suggesting less efficient coherence transfer from Cγ to Cδ under the strong coupling regime.

We also considered the maximum errors in $^{1}D_{CH}$ that could arise from two sources: the

presence of $^2D_{C-H3}$ couplings between the methine carbon and methyl protons in the aligned state, and the effect of differential relaxation rates between in-phase ($C\gamma_x$) and anti-phase ($2H\gamma_zC\gamma_y$) terms during coherence transfer.

First, two-bond dipolar couplings between the methine carbon and the six methyl protons (three from each methyl group), $^2D_{C-H3}$, in the aligned state could modulate the signal as a product of six cosine functions. As a consequence of fast methyl group rotation, the $^2D_{C-H3}$ RDC is reduced by a factor of $P_2(\cos\theta) = 0.67$ ($\theta = 28.1°$) relative to that of a static ^{13}C–^1H vector in the Cβ–Cγ direction for Leu and Cα–Cβ direction for Val. The distance (2.15 Å) between Leu Cγ and Hδ and between Val Cβ and Hγ is unaffected by methyl group rotation, and approximately twice as long as the C–H bond length (1.08 Å). As the RDC is proportional to the inverse cube of the distance, it follows that the maximum value of the $^2D_{C-H3}$ RDC is ~1/12 that of a one bond C–H RDC (i.e. ~6 Hz in the current study where $D_a^{CH} = -36$ Hz). Synthetic data points were generated for $^1J_{C\gamma-H\gamma} = 125$ Hz, in the presence of cosine modulation arising from six $^2J_{\gamma-H\delta}$ couplings, each set to a value of 6 Hz. The synthetic data were fit to a sinusoidal curve and the resulting J value was only 0.7 Hz larger than the true value of $^1J_{C\gamma-H\gamma}$. (i.e. the potential error from this source is smaller than the experimental error). Since all six C_γ–H_δ dipolar couplings cannot reach their maximum value simultaneously, the average $<^2J_{C\gamma-H\delta}>$ coupling will always be less than 6 Hz. One can therefore conclude that any error arising from $^2D_{C-H3}$ RDCs to the observed one-bond C–H methine coupling in the aligned state is negligible.

Second, differential relaxation for the in-phase ($C\gamma_x$) and anti-phase ($2H\gamma_zC\gamma_y$) terms could also potentially introduce additional errors in the measured $^1J_{CH}$ values. The scaling of the signal due to relaxation during the period between points *a* and *b* in the J-modulated HCCH-COSY pulse sequence (Figure 3) can be approximated by $\exp(-R_{ave}\cdot 2\tau_2)$, where R_{ave} is the phenomenological average of the relaxation rates R_{in} and R_{anti} for the $C\gamma_x$ and $2H\gamma_zC\gamma_y$ terms, respectively, defined as:

$$R_{ave} = \varepsilon R_{anti} + (1-\varepsilon)R_{in} \qquad (3)$$

where ε corresponds to the net fraction of the anti-phase term during the course of coherence transfer ($0 < \varepsilon < 1$). Therefore, the relaxation effect is given by $\exp(-R_{in}\cdot 2\tau_2)\exp\{-\varepsilon(R_{anti} - R_{in})\cdot 2\tau_2\}$. The first exponential term is constant; the second exponential term, however, is different for each Δ_1 time point in the J-modulation experiment since the value of ε depends on Δ_1. The difference in relaxation rates between the in-phase and anti-phase components is due to ^1H–^1H dipolar relaxation specific to the latter and is approximately given by (Cavanagh et al., 1995):

$$R_{anti} - R_{in} = \frac{1}{60}\left(\frac{\mu_0}{4\pi}\right)\hbar^2\gamma_H^4\tau_c\sum_k r_k^{-6} \qquad (4)$$

where r_k is the ^1H–^1H distance from the proton nucleus of the anti-phase term. Obviously, the difference is reduced by deuteration of the protein sample. In the present study, the main contribution for Leu $^1H\gamma$ and Val $^1H\beta$ proton nuclei will arise from intra-residue ^1H–^1H interactions with methyl protons. Taking this into account, the value of the second exponential term is very close to unity for $2\tau_2 = 7.8$ ms and the lower limit is estimated to be 0.99. Thus, the errors caused by variations in ε are negligible.

For IIA^{Chb*} we have obtained methine C–H RDCs for 14 out of 16 Leu residues and 4 out of 6 Val residues (Table 1). The cross-peaks for Leu61 and Leu107 were too weak in the aligned state to obtain reliable coupling constants. We were able to measure the Cγ–Hγ RDC for Leu85 despite the fact that no cross-peak to the Hγ resonance was observed in the 3D ^{15}N-separated NOE spectrum. Val methyl proton chemical shifts are generally more poorly dispersed than those of Leu and we could not obtain Cβ–Hβ RDCs for Val21 and Val88 due to spectral overlap.

The methine C–H RDCs of Leu and Val are very sensitive to subtle variations in side-chain conformation. For a perfectly staggered Leu side-chain in an idealized t/g^+ rotamer, the Cγ–Hγ bond vector is parallel to its own Cα–C′ bond vector; for an ideal g^-/t rotamer, the Cγ–Hγ bond is parallel to its own backbone N–Cα bond vector which is also parallel to the Cα—C′ bond vector of the preceding residue. Thus, in the idealized case the Leu C_γ–H_γ RDC should be equal to the normalized (scaled by gyromagnetic ratio and bond length) backbone Cα–C′ RDC of either its own or the preceding residue. As side-chain rotamers, however, are rarely perfectly staggered, the

normalized RDCs for Leu Cγ–Hγ and Cα–C′ are often not equal (Table 1). Similar relationships hold for Val: the Cβ–Hβ bond vector is parallel to its own Cα–C′ vector for $\chi_1 = +60°$, parallel to the Cα–C′ bond vector of the preceding residue for $\chi_1 = -60°$, and parallel to its own Cα–Hα bond vector for $\chi_1 = 180°$. Clearly, the orientational information afforded by the side-chain methine C–H RDCs of Leu and Val can be used to accurately refine their side-chain conformations in a structure calculation.

Impact of Val and Leu methine side-chain C–H RDCs in NMR structure refinement

The structure of the 34-kDa IIA^{Chb*} trimer was calculated by simulated annealing using the previously reported experimental restraints (Tang et al., 2005) supplemented by the Leu/Val methine side-chain C–H RDCs and the Leu side-chain torsion angle restraints from the present study (with ranges of $\pm 20°$ for χ_1 and $\pm 30°$ for χ_2). Three sets of calculations, each comprising 100 simulated structures, were carried out: (i) with the methine C–H RDCs represented by a harmonic potential; (ii) with the methine C–H RDCs represented by a half-harmonic potential ($E_{\text{half}}^{\text{RDC}}$) in which the restraint is satisfied if the absolute value of the calculated RDC (D_{calc}) is equal to or larger than the absolute value of the observed RDC (D_{obs}) (Ottiger et al., 1998):

$$E_{\text{half}}^{\text{RDC}} = \begin{cases} k(D_{\text{obs}} - D_{\text{calc}})^2 & \text{if } |D_{\text{calc}}| < |D_{\text{obs}}| \\ 0 & \text{if } |D_{\text{calc}}| \geq |D_{\text{obs}}| \end{cases} \quad (5)$$

(where k is the force constant); and (iii) a control set with no methine C–H RDC restraints. The force constant used for the C–H RDCs (normalized to the N–H RDCs) was 0.5 kcal mol^{-1} Hz^{-2} relative to a force constant of 1.0 kcal mol^{-1} Hz^{-2} for the N–H RDCs. These force constants are chosen to reflect the experimental error in the RDC measurements. In the absence of methine C–H RDC restraints, the r.m.s. difference between observed and calculated values for the methine C–H RDCs is 18.8 ± 1.5 Hz, approximately an order of magnitude larger than the measurement error, corresponding to a dipolar coupling R-factor (R_{dip}; Clore and Garrett, 1999) of $40.7 \pm 3.2\%$. Upon refinement of the methine C–H RDCs using a harmonic potential, the r.m.s. difference between observed and calculated values is reduced to 0.96 ± 0.11 Hz which is comparable to the experimental uncertainty and corresponds to a R_{dip} value of $2.1 \pm 0.2\%$. All the experimental restraints are satisfied within their specified errors and the introduction of the Val/Leu methine C–H RDCs does not affect the agreement with the other experimental restraints or the quality of the backbone structure (as ascertained by the percentage of residues in the most favored region of the Ramachandran map which exceeds 90%). Thus, satisfying the methine C–H RDCs can be achieved without introducing structural distortions of any kind by relatively small changes (<17°) in the Val and Leu side-chain torsion angles (Table 2). The overall r.m.s. difference between the average values of the Val and Leu side-chain torsion angles obtained with (using a harmonic potential) and without the Val/Leu methine C–H RDCs is 6.7°, ranging from 0° for the χ_2 of Leu66 to 16.5° for the χ_2 of Leu24. Larger changes would not be expected, particularly as the torsion angle database potential of mean force[30] is included in the refinement target function and in the case of high resolution crystal structures the vast majority of side-chains lie within $\pm 15°$ of the ideal rotamers (Conformational Angle Database at http://cluster.physics.iisc.ernet.in/cadb).

In the absence of the methine C–H RDCs, certain Leu χ_1/χ_2 combinations, within the limits set by the loose torsion angle restraints, are energetically favored by the non-bonded interaction terms, which include a torsion angle database potential of mean force (Clore and Kuszewski, 2002). Consequently, several χ_1/χ_2 clusters that satisfy the existing experimental restraints are observed in a χ_1/χ_2 plot (Figure 5a and 5b, green circles). Since both the torsion angle and NOE-derived distance restraints are semi-quantitative in nature, the introduction of quantitative methine C–H RDC harmonic restraints increases the precision with which the Leu side-chain conformations are determined by reducing the number of χ_1/χ_2 clusters to a single narrow cluster (Figure 5a and 5b, red circles, and Table 2). The exact location of the χ_1/χ_2 cluster obtained in the presence of the methine C–H RDCs may not necessarily overlap with those observed in the absence of the methine C–H RDCs, but in most cases the cluster obtained with the methine C–H RDCs is closer to the

Table 2. Side-chain torsion angles for Val and Leu residues in IIA^{Chb*}

	Side-chain torsion angles (deg.)[a]		
	No methine C–H RDCs	Refinement with methine C–H RDCs	
		Half-harmonic potential	Harmonic potential
Valine (χ_1)			
V20	173.4 ± 1.5	172.0 ± 1.0	172.4 ± 0.6
V21	168.5 ± 1.1	b	b
V67	171.2 ± 1.4	169.0 ± 0.8	170.1 ± 1.0
V83	43.8 ± 119.4	c	37.3 ± 118.4
V86	169.0 ± 2.4	157.7 ± 0.7	158.0 ± 0.6
V88	169.7 ± 1.1	b	b
Leucine (χ_1/χ_2)			
L17	−57.9 ± 5.3/176.7 ± 3.1	−52.5 ± 2.0/−175.4 ± 3.1	−53.1 ± 2.5/−176.3 ± 3.2
L24	−72.9 ± 3.9/170.9 ± 0.8	−62.8 ± 0.5/−172.8 ± 0.5	−62.4 ± 1.1/−172.6 ± 0.6
L34	−70.5 ± 2.3/168.6 ± 3.5	−73.9 ± 4.2/160.9 ± 3.8	−71.9 ± 2.7/163.0 ± 0.8
L39	179.4 ± 1.4/59.1 ± 1.9	176.7 ± 0.5/56.1 ± 0.3	176.7 ± 0.5/56.1 ± 0.3
L61	−71.0 ± 5.1/168.1 ± 7.1	b	b
L66	−78.5 ± 1.2/168.5 ± 5.4	−78.1 ± 1.4/170.9 ± 0.7	−78.0 ± 0.7/168.5 ± 1.2
L71	−69.4 ± 4.2/166.9 ± 5.9	−63.0 ± 0.6/177.2 ± 0.9	−63.1 ± 0.6/176.9 ± 0.9
L85	−46.1 ± 74.4/95.8 ± 90.9	c	−22.4 ± 85.3/42.4 ± 104.7
L87	−70.5 ± 4.1/170.6 ± 2.1	−69.4 ± 2.4/172.3 ± 1.2	−69.8 ± 2.7/171.8 ± 0.8
L92	170.3 ± 1.4/54.1 ± 0.6	170.3 ± 1.1 / 54.0 ± 0.5	170.6 ± 1.1 / 54.2 ± 0.5
L94	−71.8 ± 5.2/168.8 ± 4.7	−64.7 ± 1.1/−179.6 ± 0.6	−64.9 ± 1.1/−179.6 ± 0.5
L99	−174.6 ± 8.8/70.4 ± 14.2	−177.8 ± 5.1/65.7 ± 11.2	179.2 ± 0.4/59.0 ± 0.5
L103	−67.9 ± 1.2/168.2 ± 7.2	−65.0 ± 0.9/178.7 ± 0.7	−64.8 ± 1.0/178.8 ± 0.8
L107	−74.9 ± 5.4/161.9 ± 8.5	b	b
L110	−78.4 ± 2.4/169.0 ± 5.8	−80.1 ± 0.7/160.4 ± 5.6	−79.4 ± 0.5/166.7 ± 0.7
L114	−70.4 ± 5.3/167.5 ± 6.2	−63.4 ± 4.8/177.0 ± 1.7	−62.9 ± 4.7/177.1 ± 1.7

[a]For each calculation, the values reported represent the mean and standard deviations derived from an ensemble of 100 simulated annealing structures. The average torsion angle values found in the high-resolution X-ray structure database (≤ 1.8 Å resolution, crystallographic *R*-factor ≤ 18% and side-chain *B*-factor ≤ 20 $Å^2$) are as follows: 175.6 ± 6.4°, −62.0 ± 6.7° and 65.8 ± 7.8° for Val χ_1 in the *t*, g^- and g^+ rotamers, respectively (total of 5434 examples); 180.7 ± 7.8°/62.8 ± 6.6° and −64.6 ± 7.0°/174.2 ± 7.7° for Leu χ_1/χ_2 in the t/g^+ and g^-/t rotamers, respectively (6040 examples from Conformational Angle Database at http://cluster.physics.iisc.ernet.in/cadb).

[b]As the side-chain methine C–H RDCs were not measured for Val21, Val88, Leu61 and Leu107, only the torsion angles for structures calculated without the side-chain RDC restraints are listed.

[c]The side-chains of Val83 and Leu85 are highly mobile and rotamer averaged. As a result their side-chain methine C–H RDCs are close to zero (cf. Table 1). Structures were only calculated applying these methine C–H RDCs in the calculations with the harmonic potential. However, the side-chain torsion angle distributions for Val83 and Leu85 obtained with the inclusion of the side-chain methine RDC restraints are still very broad and do not converge to a single rotamer, yielding similar statistics to those obtained in the absence of side-chain RDC restraints.

statistical average of χ_1/χ_2 torsion angles derived from high-resolution crystal structures (resolution ≤ 1.8 Å, crystallographic *R*-factor ≤ 18% and side-chain *B*-factor ≤ 20 $Å^2$; Conformational Angle Database at http://cluster.physics.iisc.ernet.in/cadb). For example, the side chain conformational space sampled by Leu99 in the structures refined with methine C–H RDC restraints is narrowed down to a single tight cluster with χ_1 and χ_2 torsion angles in the range 179.2 ± 0.4° and 59.0 ± 0.5°, respectively. These values compare to the average values of 180.7 ± 7.8° and 62.8 ± 6.6°, respectively, found for the t/g^+ conformation in the high-resolution X-ray structure database (Conformational Angle Database at http://cluster.physics.iisc.ernet.in/cadb).

In addition to carrying out calculations using a harmonic potential for the methine C–H RDCs,

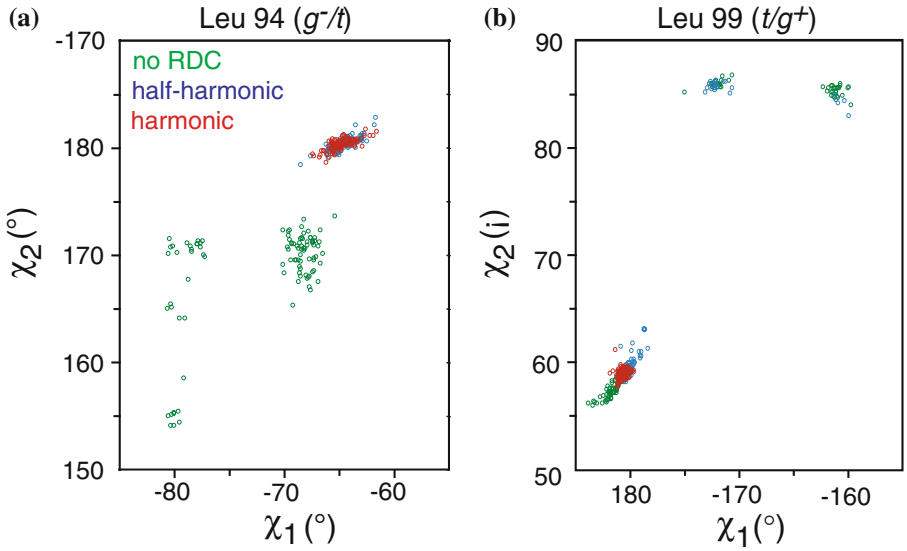

Figure 5. χ_1/χ_2 distribution for (a) Leu94 and (b) Leu99. The results for three sets of calculations, each comprising 100 simulated annealing structures, are shown: (i) no side-chain methine C–H RDCs (green), (ii) side-chain methine C–H RDCs represented by a half-harmonic potential (blue); and (iii) methine C–H RDCs represented by a harmonic potential (red).

we also carried out a set of calculations with a half-harmonic potential representation (Eq. 5). This type of potential takes into account motional effects within a given rotamer state since significant angular wobbling (≥30°) will generally result in a decrease in the value of the observed RDC (Ottiger et al., 1998). In most cases, the harmonic and half-harmonic potentials yield essentially identical results with the Leu χ_1/χ_2 torsion angles clustering in overlapping areas of the χ_1/χ_2 plot (Table 2 and Figure 5a). Accordingly, the calculated values of the methine C–H RDCs using the half-harmonic potential are very close to the observed values, as well as to the calculated values obtained with the harmonic potential, even though the calculated RDCs with the half-harmonic potential can be much larger than the observed values without paying any energy penalty. By plotting the calculated RDC values obtained with the half-harmonic potential versus the observed values, the average order parameter S can be derived from the slope, which is very close to 1 (Figure 6a), suggesting the Leu side-chains are relatively rigid.

For several residues, including Leu34, Leu99 and Leu110, the harmonic RDC potential yields more accurate structures by eliminating some bad χ_1/χ_2 clusters obtained with the half-harmonic potential. For example, Leu99 displays the largest difference between the Cγ–Hγ RDC calculated with the half-harmonic potential and the observed value (Figure 6a). In the absence of the Cγ–Hγ RDC restraint, the χ_1/χ_2 torsion angles of Leu99 are clustered in three regions, two of which with relatively low occupancies are very close to the edge of the side-chain torsion angle restraints (Figure 5b, green dots). The introduction of the Cγ–Hγ RDC restraint for Leu99 in the form of a half-harmonic potential does not eliminate any of the minor χ_1/χ_2 clusters, although their occupancy is decreased somewhat (Figure 5b, blue dots). The calculated value of the Cγ–Hγ RDC obtained for the major cluster is very close to the observed value, but those calculated for the two minor clusters are more than three times larger. The additional conformations are very unlikely since the side-chain of Leu99 is involved in the formation of the coiled-coil trimer of IIA^{Chb*} and the Cγ–Hγ order parameter S would otherwise be less than 0.3. With the harmonic potential, however, the χ_1/χ_2 clusters with unusually large calculated RDCs are completely eliminated (Figure 5b, red dots). The remaining χ_1/χ_2 cluster is very close to the statistical average for the t/g^+ conformation found in the high-resolution X-ray structure database (Figure 5b, red dots, and Table 2). From a structural perspective, the side-chains of Leu99 from each subunit of the trimer are more optimally packed in

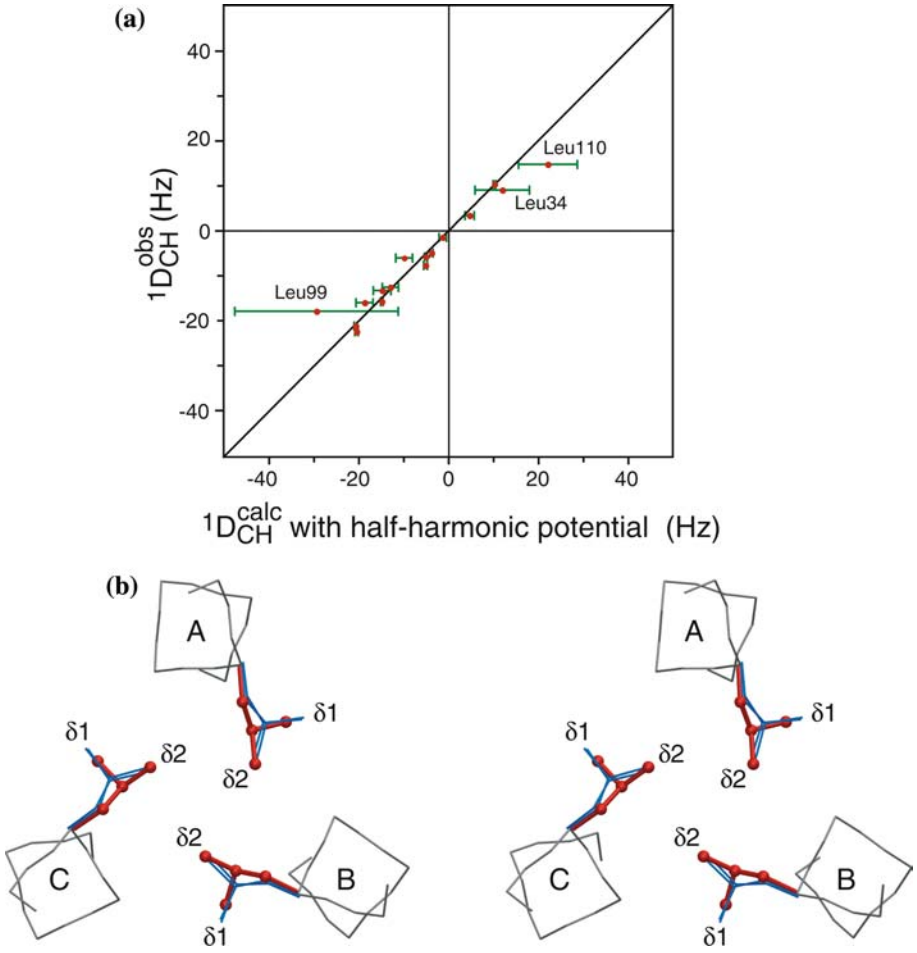

Figure 6. (a) Plot of calculated RDCs for the side-chain methine C–H bond vectors of Leu and Val obtained using the half-harmonic potential versus the observed RDC values (excluding Val83 and Leu85 which are disordered). The mean calculated values from 100 simulated annealing structures are shown as *red* dots, and the standard deviations of the calculated RDCs are shown as *green* bars. In the case of Leu34, Leu99 and Leu110, the half-harmonic potential does not efficiently restrict the side-chain conformation, resulting in several discrete χ_1/χ_2 clusters and a concomitant broad distribution of calculated RDCs. (b) Stereoview displaying the side-chains of the three-symmetry-related Leu99 residues at the trimer interface of IIA^{Chb*}. Three representative side chain conformations corresponding to the three clusters shown in Figure 5b are shown, with the optimally staggered conformation obtained with the harmonic RDC restraints displayed as a red ball-and-sticks, and the two bad conformations obtained without RDC restraints displayed as blue sticks. The backbone for residues 98–103 from all three subunits is shown in gray.

the structures calculated with the harmonic RDC potential (Figure 6b, red ball-and-sticks). This is manifested by a significant decrease (~0.5 Å) in the intermolecular distances from the Leu99 $C\delta_2$ atoms of subunits A, B and C to the Leu99 $C\gamma$ atoms of subunits B, C and A, respectively: the average value of these distances (over an ensemble of 100 calculated structures) is 4.44 ± 0.31 Å for the structures calculated with the harmonic RDC potential versus 5.05 ± 0.14 Å and 4.91 ± 0.25 Å for the two alternative clusters observed in the structures calculated without methine C–H RDCs.

Clearly, some Leu and Val side-chains may be disordered. This is the case, for example, for Val83 and Leu85 which are located in a long, highly flexible loop connecting helices 2 and 3. Quantitative J-correlation experiments (Bax et al., 1994) indicate that these two side-chains are rotamer averaged (Tang et al., 2005). In accordance with this finding, the observed methine C–H RDC values for these two residues are rather small (Table 1), which also suggests the presence of significant motion and subsequent scaling by a low order parameter. Inclusion of the methine C–H

RDCs for these two residues in the structure calculation does not lock the side-chains of Val83 and Leu85 into any particular rotamer nor narrow the distribution of the side-chain torsion angles (Table 2). Thus, in the absence of side-chain torsion angle restraints, the side-chain methine C–H RDC is not sufficient to define a unique side-chain conformation and therefore will not over-restrain the side-chain in an incorrect conformation.

Concluding remarks

In this paper we have presented a novel method for accurately determining the side-chain conformations of Leu and Val based on the use of [$^{13}C_5$]-α-ketoisovalerate as a biosynthetic precursor to selectively protonate the methine and methyl side-chain groups of Leu and Val in a uniformly $^{15}N/^{13}C/^{2}H$ labeled background. The advantages of this labeling scheme are demonstrated by structure refinement of $IIA^{Chitobiose}$, a 34-kDa trimeric phosphotransferase protein. First, the side-chain χ_1/χ_2 rotamers of Leu (t/g^+ or g^-/t) can be readily ascertained from a simple 3D ^{15}N-separated NOE spectrum based on the pattern of intraresidue and sequential interresidue NOEs involving the Hγ and backbone amide protons free from spectral overlap or spin-diffusion. The Hγ(i) proton is closer to H_N(i) for the g^-/t rotamer but closer to $H_N(i+1)$ for the t/g^+ rotamer. The availability of these rotamer assignments eliminates the need to obtain *a priori* stereospecific assignment for Leu prochiral methyl groups, which can be established during the course of structural calculations using ambiguous restraints for the non-sequential NOEs involving Leu and Val methyl groups. Second, accurate measurement of RDCs can be obtained for the Leu Cγ–Hγ and Val Cβ–Hβ bond vectors without complications arising from resonance overlap and passive couplings in a fully protonated sample. Incorporation of the one-bond methine side-chain C–H RDCs into the structure calculation, in conjunction with loose torsion angle restraints, significantly improves both the precision and accuracy with which the coordinates of Leu and Val side-chains (not rotamer averaged) are determined. It should be noted that our approach makes the simplifying assumption of a single rotamer for Leu and Val side-chains that are buried either within the protein interior or at an intermolecular interface, and does not take into account the possible existence of minor rotameric states of Leu and Val. The observation that the C–H RDCs can be readily satisfied within the confines of this assumption and that the resulting side-chain torsion angles generally become closer to the average values observed in the high-resolution crystal structure database, suggests that the application of Occam's Razor is perfectly reasonable and for most purposes minor rotameric states of Leu and Val side-chains do not need to be invoked. In those cases where rotameric averaging is present and no single rotameric state can be identified from the NOE data, the methine C–H RDCs do not lock the side-chains into any unique conformation (cf. Val 83 and Leu85). In cases where a minor rotameric state may be present with an occupancy of 10% or less, the contribution of the minor state to the observed C–H RDC will usually be negligible and within the uncertainties of the measurement. If the contribution of the minor rotameric state to the observed methine C–H RDC is indeed significant, this will be manifested by significant deviations in the values of the resulting torsion angles away from their expected values (i.e. skewed rotamers).

In an earlier report, [$^{13}C_5$, 3–$^{2}H_1$]-α-ketoisovalerate, a compound that is derived from [$^{13}C_5$]-α-ketoisovalerate, was used to selectively protonate only the methyl groups of Leu and Val (Goto et al., 1999). This type of labeling scheme has proven to be extremely powerful in the study of larger proteins since perdeuteration lowers the proton density and slows the overall transverse relaxation rates, while fast rotation and three-fold degeneracy give the methyl protons a further edge in relaxation properties (Gardner and Kay, 1998). In favorable cases it is possible to determine a complete high-resolution three-dimensional protein structure based solely on NOEs involving methyl and backbone amide groups combined with torsion angle restraints and backbone RDCs (Tang et al., 2005). Since additional protonation of the methine proton has little effect on the favorable relaxation properties of the methyl groups of Leu and Val, and since the current labeling scheme also permits accurate determination of the side-chain conformations of Leu and Val, we suggest that labeling with [$^{13}C_5$]-α-ketoisovalerate rather than [$^{13}C_5$, 3–$^{2}H_1$]-α-ketoisovalerate may be

the method of choice for structure determination of medium to larger sized proteins by NMR. Thus, labeling with [$^{13}C_5$]-α-ketoisovalerate together with [$^{13}C_4$, 3,3–$^{2}H_2$]-α-ketobutyrate to additionally selectively protonate the δ-methyls of Ile, will generate a single U-[^{15}N/^{13}C/^{2}H]/[^{1}H-methyl-Ile/Leu/Val]/[^{1}H-methine-Leu/Val] sample that can be used to carry out almost all of the experiments required for protein structure determination of larger proteins (i.e. TROSY-based sequential through-bond correlation experiments for backbone and side-chain assignments, experiments for measuring backbone RDCs, NOE experiments for detecting through-space interactions between NH, Ile/Leu/Val methyl and Leu/Val methine groups, as well as the Leu/Val methine C–H RDC experiment reported in this paper). For very large proteins (> 70–80 kDa) it may be advantageous to use [$^{13}C_5$, 4–$^{2}H_3$]-α-ketoisovalerate rather than [$^{13}C_5$, 4–$^{2}H_3$, 3–$^{2}H_1$]-α-ketoisovalerate (Tugarinov and Kay, 2004) so that protonation at the methine position in addition to non-stereospecific protonation at only one of the methyl groups is obtained. Such a labeling scheme will enhance the relaxation properties of the protonated methyl group, albeit at the expense of losing a factor of two in signal intensity, and therefore only becomes beneficial for very high molecular weight systems. Since the methyl groups of Leu and Val are involved in extensive non-bonded contacts, the delineation of the side-chain conformations of Leu and Val has significant impact on the accuracy with which the fold of larger proteins can be determined using minimal NOE datasets based primarily on NOEs involving methyl groups (Tugarinov et al., 2005).

Acknowledgements

We thank Frank Delaglio for assistance with data analysis using NMRPipe/nmrDraw. This study utilized the high-performance computational capabilities of the Biowulf PC/Linux cluster at the National Institutes of Health, Bethesda, MD (http://biowulf.nih.gov). This work was supported in part by the AIDS Targeted Antiviral Program of the Office of the Director of the National Institutes of Health (to G.M.C.).

References

Al-Hashimi, H.M., Bolon, P.J. and Prestegard, J.H. (2000) *J. Magn. Reson.* **142**, 153–158.
Bax, A., Kontaxis, G. and Tjandra, N. (2001) *Methods Enzymol.* **339**, 127–174.
Bax, A., Max, D. and Zax, D. (1992) *J. Am. Chem. Soc.* **114**, 6923–6925.
Bax, A., Vuister, G.W., Grzesiek, S., Delaglio, F., Wang, A.C., Tschudin, R. and Zhu, G. (1994) *Methods Enzymol.* **239**, 79–105.
Betts, M.J. and Sternberg, M.J.E. (1999) *Protein Eng.* **12**, 271–283.
Bruschweiler, R. and Case, D.A. (1994) *Prog. NMR Spectrosc.* **26**, 27–58.
Cai, M.L., Huang, Y. and Clore, G.M. (2001) *J. Am. Chem. Soc.* **123**, 8642–8643.
Cavanagh, J., Fairbrother, W.J., Palmer, A.G. and Skelton, N.J. (1995) *Protein NMR Spectroscopy: Principles and Practice*, Chapter 7. Academic Press, London, UK, pp. 410–531.
Chou, J.J. and Bax, A. (2001) *J. Am. Chem. Soc.* **123**, 3844–3845.
Clore, G.M. and Garrett, D.S. (1999) *J. Am. Chem. Soc.* **121**, 9008–9012.
Clore, G.M. and Gronenborn, A.M. (1989) *CRC Crit. Rev. Biochem. Mol. Biol.* **24**, 479–564.
Clore, G.M. and Kuszewski, J. (2002) *J. Am. Chem. Soc.* **124**, 2866–2867.
Clore, G.M. and Schwieters, C.D. (2004) *J. Am. Chem. Soc.* **126**, 2923–2938.
Clore, G.M., Starich, M.R. and Gronenborn, A.M. (1998) *J. Am. Chem. Soc.* **120**, 10571–10572.
Cornilescu, G., Delaglio, F. and Bax, A. (1999) *J. Biomol. NMR* **13**, 289–302.
Delaglio, F., Grzesiek, S., Vuister, G.W., Zhu, G., Pfeifer, J. and Bax, A. (1995) *J. Biomol. NMR* **6**, 277–293.
Evenas, J., Mittermaier, A., Yang, D.W. and Kay, L.E. (2001) *J. Am. Chem. Soc.* **123**, 2858–2864.
Gardner, K.H. and Kay, L.E. (1998) *Ann. Rev. Biophys. Biomol. Struct.* **27**, 357–406.
Goto, N.K., Gardner, K.H., Mueller, G.A., Willis, R.C. and Kay, L.E. (1999) *J. Biomol. NMR* **13**, 369–374.
Grishaev, A. and Bax, A. (2004) *J. Am. Chem. Soc.* **126**, 7281–7292.
Hajduk, P.J., Augeri, D.J., Mack, J., Mendoza, R., Yang, J.G., Betz, S.F. and Fesik, S.W. (2000) *J. Am. Chem. Soc.* **122**, 7898–7904.
Hansen, M.R., Mueller, L. and Pardi, A. (1998) *Nat. Struct. Biol.* **5**, 1065–1074.
Higman, V.A., Boyd, J., Smith, L.J. and Redfield, C. (2004) *J. Biomol. NMR* **30**, 327–346.
Hu, J.S. and Bax, A. (1997) *J. Biomol. NMR* **9**, 323–328.
Karplus, A. (1996) *Protein Sci.* **5**, 1406–1420.
Kay, L.E., Xu, G.Y., Singer, A.U., Muhandiram, D.R. and Forman-Kay, J.D. (1993) *J. Magn. Reson. Series B* **101**, 333–337.
Konrat, R., Muhandiram, D.R., Farrow, N.A. and Kay, L.E. (1997) *J. Biomol. NMR* **9**, 409–422.
Kontaxis, G. and Bax, A. (2001) *J. Biomol. NMR* **20**, 77–82.
Kuszewski, J., Gronenborn, A.M. and Clore, G.M. (1996) *Protein Sci.* **5**, 1067–1080.

Kuszewski, J., Gronenborn, A.M. and Clore, G.M. (1999) *J. Am. Chem. Soc.* **121**, 2337–2338.
Lo Conte, L., Chothia, C. and Janin, J. (1999) *J. Mol. Biol.* **285**, 2177–2198.
Mittermaier, A. and Kay, L.E. (2001) *J. Am. Chem. Soc.* **123**, 6892–6903.
Najmanovich, R., Kuttner, J., Sobolev, V. and Edelman, M. (2000) *Proteins* **39**, 261–268.
Nilges, M., Gronenborn, A.M., Brünger, A.T. and Clore, G.M. (1988) *Protein Eng.* **2**, 27–38.
Ottiger, M., Delaglio, F., Marquardt, J.L., Tjandra, N. and Bax, A. (1998) *J. Magn. Reson.* **134**, 365–369.
Permi, P. (2001) *J. Magn. Reson.* **153**, 267–272.
Permi, P., Rosevear, P.R. and Annila, A. (2000) *J. Biomol. NMR* **17**, 43–54.
Peruvshin, K., Riek, R., Wider, G. and Wüthrich, K. (1997) *Proc. Natl. Acad. Sci. USA* **94**, 12366–12371.
Prestegard, J.H., Al-Hashimi, H.M. and Tolman, J.R. (2000) *Quart. Rev. Biophys.* **33**, 371–424.
Schwieters, C.D. and Clore, G.M. (2001a) *J. Magn. Reson.* **149**, 239–244.
Schwieters, C.D. and Clore, G.M. (2001b) *J. Magn. Reson.* **152**, 288–302.
Schwieters, C.D., Kuszewski, J., Tjandra, N. and Clore, G.M. (2003) *J. Magn. Reson.* **160**, 66–74.
Sibille, N., Bersch, B., Coves, J., Blackledge, M. and Brutscher, B. (2002) *J. Am. Chem. Soc.* **124**, 14616–14625.
Tang, C., Williams, D.C., Ghirlando, R. and Clore, G.M. (2005) *J. Biol. Chem.* **280**, 11770–11780.
Tjandra, N. and Bax, A. (1997) *Science* **278**, 1111–1114.
Tjandra, N., Omichinski, J.G., Gronenborn, A.M., Clore, G.M. and Bax, A. (1997) *Nat. Struct. Biol.* **4**, 732–738.
Tolman, J.R., Flanagan, J.M., Kennedy, M.A. and Prestegard, J.H. (1995) *Proc. Natl. Acad. Sci. USA* **92**, 9297–9283.
Tugarinov, V. and Kay, L.E. (2004) *J. Biomol. NMR* **28**, 165–172.
Tugarinov, V., Choy, W.Y., Orekhov, V.Y. and Kay, L.E. (2005) *Proc. Natl. Acad. Sci. USA* **102**, 622–627.
Vögeli, B., Kovacs, H. and Peruvshin, K. (2004) *J. Am. Chem. Soc.* **126**, 2414–2420.
Wang, G., Louis, J.M., Sondej, M., Seok, Y.-J., Peterkofsky, A. and Clore, G.M. (2000) *EMBO J.* **19**, 5635–5649.
Wüthrich, K. (1986) *NMR of Proteins and Nucleic Acids* John Wiley & Sons, New York.
Yang, D., Venters, R.A., Mueller, G.A., Choy, W.Y. and Kay, L.E. (1999) *J. Biomol. NMR* **14**, 333–343.